Correction of magnification in vertical dual-exposure panoramic radiography

Hideaki Kimoto

Nihon University Graduate School of Dentistry,

Major in Oral and Maxillofacial Radiology

(Directors: Prof. Yoshinori Arai and Assoc. Prof. Kunihito Matsumoto)

Contents

This thesis is based on the article listed below with additional data.

Kimoto H, Asakura S, Sasaki T, Dezawa K, Amemiya T, Matsumoto K, Arai Y (2023) Vertical magnification correction in vertical dual-exposure panoramic radiography. J Oral Sci (in press)

Summary

Panoramic radiography (PR) is an imaging method that scans the dental arch using slit imaging and tomography. PR has the disadvantage of overlapping ghost images of the cervical vertebrae and intervertebral space in the incisal region. When a radiolucent ghost image overlaps with the apex of the incisor, it is difficult to distinguish a radiolucent ghost image from a periapical lesion. To solve the problem of ghost images of the intervertebral space overlapping the incisors, the vertical dual-exposure PR method was proposed. In this method, the first PR is taken in a conventional position, and the second is taken with the X-ray focus raised by 5 to 20 mm. The two PR images taken with the X-ray focus at different heights are then merged by the least squares method. However, when the X-ray focus is raised, the image of the incisors is vertically distorted because of the change in the angle of the incident X-ray beam to the incisors compared with the conventional position. Alternatively, the length of the incisors on PR depends on the tilt of the incisors in the labio-palatal direction because the magnification of the incisor varies as the distance between the incisal edge and the X-ray focus differs from the distance between the apex of the incisor and the X-ray focus in both conventional PR and vertical dual-exposure PR. These effects may cause distortion of the incisors in the vertical direction when the images of the incisors are merged in vertical dual-exposure PR. However, this effect has not been elucidated. The aims of this study were to clarify the magnification error caused by the tilt of the incisor and the elevation of the X-ray focus position, and to assess the verification effect of magnification correction in the vertical direction when performing vertical dual-exposure PR.

A steel ball phantom was used as the object. Twenty-six steel balls with a diameter of 0.5 mm were embedded in an acrylic plate and were arranged at equal intervals along a 50-mm-long straight line. The position of 30 mm from the top of the uppermost steel ball was set as the center of rotation when tilting. PR images were taken

at different heights (0, 5, 10, 15, and 20 mm) and tilt angles (0°, 10°, 20°, and 30°) to evaluate vertical magnification in each condition. Using an original software with the least squares method, the magnification of the vertical direction of the PR image compared with the original PR image taken at X-ray focus height of 0 mm at each tilt angle was calculated as the measured magnification value (MMV) at each height position and tilt angle. The difference between the theoretical magnification value (TMV) and MMV was calculated as the error. Spearman's rank correlation coefficient was calculated between TMV and MMV. The subtracted and merged images were created with the original PR image taken at X-ray focus heights of 0 mm and the PR image after magnification correction in the vertical direction with the MMV taken at each height of the X-ray focus. This process is referred to as the vertical magnification correction. Pixel values in the region of interest of the subtracted PR images before and after vertical magnification correction were measured. Standard deviations (SD) of the pixel value were calculated.

For the human head phantom with cervical vertebrae, subtracted and merged PR images were obtained from the two PRs taken at X-ray focus heights of 0 mm and 20 mm. SD of the pixel value in the region of interest of the subtracted PR images were compared before and after vertical magnification correction.

The MMV decreased with increasing object tilt angle and X-ray focus height in PR. As the phantom was tilted, it expanded laterally as the upper steel ball deviated from the tomographic layer. The range of the error in the steel ball phantom was −0.35-0.30%. The Spearman's rank correlation coefficient between TMV and MMV was 0.983 ($P < 0.05$). Before vertical magnification correction, the SDs increased in correlation with both the increase in the object tilt angle and the increase in the height of the X-ray focus with the steel ball phantom. After vertical magnification correction, the SDs decreased in all conditions. In the human head phantom, vertical magnification correction improved the SD of pixel value in the region of interest from 7.113 to 6.727.

This study clearly demonstrated that vertical magnification correction improved the uniformity of pixel value of the subtracted images in the vertical dual-exposure PR method. Vertical dual-exposure PR method with vertical magnification correction has the potential to provide higher quality merged PR images than the method without correction.

Introduction

Panoramic radiography (PR) is an imaging method that scans the dental arch using slit imaging and tomography [1,2]. When imaging incisors with this method, X-rays are passed through the head from behind. The X-rays pass through the cervical vertebrae and the incisors are projected onto the detector. A tomographic layer is set on the incisor, establishing a clear image. However, because the cervical vertebrae deviate greatly from the tomographic layer, they are superimposed on the incisor as a ghost image [3-5].

The ghost images of the cervical vertebrae and intervertebral space (IVS) alternate between radio-opaque and radiolucent images in the incisal region. When a radiolucent image overlaps with the apex of the incisor, it is difficult to distinguish a radiolucent ghost image from a periapical lesion [6]. In these cases, intraoral radiographs are generally taken. However, during the Covid-19 pandemic, intraoral radiography was discouraged to prevent the spread of infection [7-10].

To solve the problem of ghost images of the IVS overlapping the incisors, Kato et al. [11] proposed the vertical dual-exposure PR method. In this method, the first PR is taken in a conventional position, and the second is taken with the X-ray focus raised by 5 to 20 mm. Raising the X-ray focus moves the position of the ghost image of the IVS downward relative to the incisors. Although the ghost image of the IVS overlaps the incisors, the position of the ghost image shifts between the first and second PR images. The two PR images taken with the X-ray focus at different heights are then merged by the least squares method. Kato et al. [11] concluded that the vertical dual-exposure PR method can reduce the negative effects of ghost images of the cervical vertebrae and IVS.

However, when the X-ray focus is raised, the image of the incisors is vertically distorted because of the change in the angle of the incident X-ray beam to the incisors compared with the conventional position. Vertical dual-exposure PR therefore provides a poor merged image when there is a large difference in the length of the incisors between the two PR images [11]. Alternatively, the length of the incisors on PR depends on the tilt

of the incisors in the labio-palatal direction because the magnification of the incisor varies as the distance between the incisal edge and the X-ray focus differs from the distance between the apex of the incisor and the X-ray focus in both conventional PR and vertical dual-exposure PR. These effects may cause distortion of the incisors in the vertical direction when the images of the incisors are merged in vertical dual-exposure PR. However, this effect has not been elucidated.

The aims of this study were 1) to clarify the magnification error caused by the tilt of the incisor and the elevation of the X-ray focus position, and 2) to assess the verification effect of magnification correction in the vertical direction when performing vertical dual-exposure PR.

Materials and Methods

Theoretical analysis

Magnification of incisors depends on the horizontal positional relationship between the X-ray focus, the object, and the detector as shown in Fig. 1. When the X-ray focus and detector are raised and/or the incisors are tilted, the magnification value also varies. When raising the X-ray focus and detector from the original position (0 mm: F_0) to H mm (F_H), object length (O_L: distance between a-point [O_a] and b-point [O_b] of the object in Fig. 1) on the detector changes from I_{F0} to I_{FH}, indicating that the length of the incisor on the detector is slightly shortened. I_{F0} and I_{FH} were calculated with the following formula (see Fig. 1):

$$I_{F0} = O_L \cos\theta \times d_{F\text{-}De}/d_{F\text{-}Ob}$$

$$I_{FH} = O_L \cos\theta \times d_{F\text{-}De}/d_{F\text{-}Ob} - H \times (d_{Oa\text{-}De}/d_{F\text{-}Oa} - d_{Ob\text{-}De}/d_{F\text{-}Ob})$$

Where abbreviations are follows: θ, tilt angle; $d_{F\text{-}De}$, horizontal distance between X-ray focus and detector; $d_{F\text{-}Oa}$, horizontal distance between X-ray focus and O_a; $d_{Oa\text{-}De}$, horizontal distance between O_a and detector; $d_{F\text{-}Ob}$, horizontal distance between X-ray focus and O_b; $d_{Ob\text{-}De}$, horizontal distance between O_b of the object and detector.

The actual values of $d_{F\text{-}De}$, $d_{F\text{-}Oa}$, $d_{Oa\text{-}De}$, and O_L were 518.0 mm, 398.5 mm, 119.5 mm, and 30.0 mm in this study, respectively. Other items were variable according to setting of H and θ. The theoretical vertical magnification of the object was 1.30 times at O_a. Finally, the theoretical magnification value (TMV) between the PR images taken at two different heights (F_0 and F_H) was calculated with the following formula:

$$TMV = I_{FH}/I_{F0}$$

$$= 1 - H/d_{F\text{-}Oa} \times \tan\theta$$

Imaging phantoms

Steel ball phantom

The steel ball phantom, which was originally made and has been used for maintenance of the PR apparatus (Fig. 2A), was used as the object. Twenty-six steel balls with a diameter of 0.5 mm were embedded in an acrylic plate and were arranged at equal intervals along a 50-mm-long straight line. The position of 30 mm from the top of the uppermost steel ball was set as the center of rotation when tilting.

Human head phantom

A human head phantom (SE-2, Osaka Kasei Co., Osaka, Japan) with cervical vertebrae was used as the object.

Imaging conditions

Veraviewepocs X550 (J. Morita Co.) was used for imaging. The exposure conditions were 60 kV, 1 mA and 15 s, with an additional filter of 0.2 mm of copper plate for the steel ball phantom. The center position was defined as a position 30-mm below the top of the uppermost steel ball. This center position was aligned to the tomographic layer with the lateral, central, and horizontal laser beam. It was then tilted from 0° to 10°, 20°, and 30° toward the X-ray focus side (Fig. 2B). PRs were also taken with the height of the X-ray focus raised from 0 mm to 5, 10, 15 and 20 mm.

For the human head phantom, the Frankfurt horizontal plane of the human head phantom was set parallel to the floor after midline positioning. The lateral laser beam for anteroposterior positioning of the tomographic layer was fixed at the left maxillary canine of the human head phantom. The exposure conditions were 80 kV, 5 mA and 15 s. Two PRs were taken with the X-ray focus at heights of 0 mm and 20 mm.

Image processing to construct subtracted and merged images

A software developed with C# (Microsoft, Redmond, WA, USA) was used to subtract and merged images by applying the least squares method [12-17]. The PR images taken at H_0 were matched to those taken at heights of 5, 10, 15, and 20 mm by tilting from 0° to 10°, 20°, and 30°. At these positions, subtracted and merged images were constructed and exported as 8-bit grayscale bitmaps.

Calculation of magnification value and vertical magnification correction

Using the software, the magnification of the vertical direction of the PR image compared with the original PR image taken at H_0 at each tilt angle was calculated as the measured magnification value (MMV) at each height position and tilt angle. The difference between the TMV and MMV was calculated as the error.

The subtracted and merged images were created with the original PR image taken at H_0 and the PR image after magnification correction in the vertical direction with the MMV taken at each height of the X-ray focus. This process is referred to as the vertical magnification correction.

For the human head phantom, subtracted and merged PR images were obtained from the two PRs taken at X-ray focus heights of 0 mm and 20 mm. Vertical magnification correction was performed with the MMV measured as above.

Densitometry of the subtracted images

Pixel values in the region of interest of the subtracted PR images of both phantoms before and after vertical magnification correction were measured using the software. The regions of interest were set to 100 × 700 pixels for the steel ball phantom and 359 × 379 pixels for the human head phantom. SDs of the pixel value were calculated.

Statistical analysis

Spearman's rank correlation coefficient was calculated between TMV and MMV using SPSS (IBM Corp., Armonk, NY, USA). A *P* value of less than 0.05 was considered to indicate a statistically significant difference.

Results

Figure 3 shows images taken with the X-ray focus at the conventional height of 0 mm and the steel ball phantom tilted at 0°, 10°, 20°, and 30°. As the phantom was tilted, it expanded laterally as the upper steel ball deviated from the tomographic layer.

Figure 4 shows an image with the X-ray focus raised by 5, 10, 15, and 20 mm at each angle of 0°, 10°, 20°, and 30°. Figure 5 shows the subtracted PR images obtained by matching the positions using the least squares method. As the tilt angle increased, the X-ray focus position also increased, and as the position of the steel ball increased, the deviation of images shown as black and white horizontal lines also increased.

Table 1 shows the theoretical and actual correction of the magnification ratio at each tilt angle and height of the X-ray focus. The maximum error was 0.30%, and the minimum was −0.35%. Figure 6 shows the regression line of the TMV and MMV obtained by the least squares method at each tilt angle and height of the X-ray focus in the steel ball phantom experiment. The Spearman's rank correlation coefficient was 0.983 ($P < 0.05$). Figure 7 shows the subtracted images between images at F_0 and images with vertical magnification correction at F_H. The matching area increased from the uncorrected image shown in Fig. 5. The merged images before and after vertical magnification correction also substantially match the merged images before vertical magnification correction (Fig. 8). Blurring in the vertical direction is significantly improved after vertical magnification correction.

PR images of the human head phantom before and after vertical magnification correction are shown in Fig. 9. A white line was observed on the incisal edge of the maxillary incisor in the subtracted PR image (Fig. 9C) before correction, but it was alleviated after correction of the magnification ratio in the vertical direction (Fig. 9D).

Before vertical magnification correction, the SDs increased in correlation with both the increase in the object tilt angle and the increase in the height of the X-ray focus in the steel ball phantom (Table 2). After vertical magnification correction, the SDs

decreased in all conditions. In the human head phantom, vertical magnification correction improved the SD of pixel value in the region of interest from 7.113 to 6.727.

Discussion

Diagnosis in the incisal region has been hindered by overlapping ghost images of cervical vertebrae and the IVS on PR images [4]. In particular, when the ghost image of the IVS overlapped the apex of the incisors, periapical lesions were sometimes difficult to diagnose. Kato et al. [11] proposed vertical dual-exposure PR as a method to reduce ghost images of the cervical vertebrae and IVS. In this method, PR images are taken twice with the X-ray focus at different heights, and these images are merged. Raising the position of the X-ray focus makes the ghost image of the IVS shift downward to the apex of the incisor. The basic principle is the same as the eccentric projection method in intraoral radiography.

A merged PR image is obtained using the least squares method so that the images of the incisor on the two PRs match. The least squares method shifts the position of the image until the minimum value of the sum of the squares of each subtracted pixel value is reached [12-17], and is used in the energy subtraction method and dual imaging plate (DIP) method. Sekiguchi et al. [17] reported that DIP intraoral radiography can reduce noise and artifacts such as scratches and dust. In DIP intraoral radiography, the front and back imaging plate images were merged. Theoretically, the geometrical positional relationship between the front and back imaging plate images is substantially the same. In fact, the imaging plate is scanned with a laser beam while moving in a longitudinal direction. It became clear that the geometric positional relationship between the first front imaging plate and the second back imaging plate images did not match because the speed of movement of the imaging plate in the long axis direction changes because of slippage. The positional relationship between the two images was improved by correcting the magnification ratio in the longitudinal direction.

The PR used in this study has a semiconductor charged coupled device as a detector, and therefore it is assumed that there are no geometrical strain changes caused by the positional relationship of the detector [18,19]. PR has the two characteristics of slit

imaging and tomography. When the object is in the tomographic layer, a sharp image can be produced where the tomographic layer coincides with the object. Alternatively, lateral direction distortion and blurring of the object images may occur outside of the tomographic layer. Therefore, the images of the steel balls that were closer to the X-ray focus than the tomographic layer are blurred and stretched in the lateral direction. For this reason, as shown by the arrow of O_b in Fig. 3, the larger the tilt angle and the higher the position of the steel ball, the more the image is stretched in the lateral direction. In contrast, when the object is outside of the tomographic layer, the projected image will be narrow in the lateral direction with blurring. Thus, the image of the steel ball located at the bottom in Fig. 3 became narrower in the lateral direction as the tilt angle increased.

There is no tomographic effect in the vertical direction in PR. The magnification ratio in the vertical direction is determined by the positional relationship between the detector, the object, and the X-ray focus, as in general radiography. Therefore, as the object becomes closer to the detector, the magnification decreases. Additionally, as the object becomes closer to the X-ray focus, the magnification increases. Therefore, as shown in Fig. 1, when the object is tilted, O_b is closer to the X-ray focus than O_a, so the magnification of O_b is greater than that of O_a. Furthermore, when the X-ray focus is raised, as shown in Fig. 1, the closer the O_b to the focus, the greater is the shifting distance than O_a. For this reason, if the X-ray focus is raised by a distance of H and the object is tilted as shown in Fig. 1, the height of the object on the detector in the vertical direction is shorter.

A PR image of an actual steel ball phantom is shown in Fig. 4. It is unclear from the image whether the vertical length is shortened. The subtracted images of the steel balls between the image at the conventional height of 0 mm and the images at heights of 5, 10, 15, and 20 mm in Fig. 5 demonstrate that the larger the tilt angle, the higher the elevation of the X-ray focus, and the closer to the upper edge of O_b from O_a as the center, the larger was the gap. The resulting gap is displayed as horizontal lines of black and white. The

merged image without vertical magnification correction in Fig. 8 demonstrates that the larger the tilt angle, the higher the elevation of the X-ray focus, and the closer the proximity to the upper edge of the steel ball, the more blurred was the image in the vertical direction. After the correction, the black and white lateral lines in the vertical direction are smaller than those in Fig. 5 before correction. Blurring in the vertical direction was also reduced in the merged image (Fig. 8). SDs decreased after vertical magnification correction, indicating improvement of uniformity of the pixel value on the subtraction images (Table 2).

In the subtracted image of the human head phantom, the position of the incisal edge of the maxillary incisor did not accurately overlap the conventional position at X-ray focus heights of 0 mm and 20 mm, and thus it was observed as a white line (Fig. 9C). This was alleviated by the correction (Fig. 9D). It seems that the vertical height caused by the tilt of the incisor has been corrected. However, in the corrected differential image, the incisal edge of the mandibular canine was observed as a white line (Fig. 9D). This may be because the incisor of the mandible is located more lingually than the incisor of the maxilla, and the degree of magnification differs from that of the maxilla. As described above, these findings establish that the images are less likely to overlap because the magnification ratio in the vertical direction differs as the tilt of the incisor and the elevation of the X-ray focus increase. Additionally, it was clarified that the method of correcting the magnification ratio in the vertical direction by the least squares method agrees well with the TMV, and that the corrected images can create significantly more accurate merged images.

However, by tilting the steel ball phantom of the object, the object was positioned outside the tomographic layer. As a result, blurring occurred. This blur did not change with this correction. It was thought that this blurring in the lateral direction could be improved by using tomosynthesis [20,21]. Because a charged coupled device was used for the sensor in this experiment, it was not possible to change the tomographic layer after

taking the PR. In PR equipped with a complementary metal-oxide semiconductor sensor, it would be possible to convert the tomographic layer by synthesizing it even after taking the PR image [21]. Future experiments should be conducted with PR with synthesizing capability.

This study showed that the tilt angle of the object in the incisal region was correlated with the amount of laterally stretched blur by changing the position of the tomographic layer and the object. In the vertical direction, image magnification was also influenced by the tilt angle of the object in the incisal region. Vertical magnification correction has the potential to improve image quality when merging panoramic radiographs in vertical dual-exposure PR, as well as to reduce the ghost imaging of the cervical vertebrae and intervertebral space. When it is necessary to obtain details of the incisors and their peripheral anatomical structures, the vertical dual-exposure PR method with vertical magnification correction could be a good choice for patients with gag reflex and severe trismus, and for pediatric patients who cannot undergo intraoral radiography, as well as under pandemics such as Covid-19.

Conclusions

1. The vertical magnification ratio decreased with increasing object tilt angle and X-ray focus height in PR.
2. The MMV calculated with the steel phantom in the vertical direction was strongly correlated with the TMV.
3. Vertical magnification correction improved the uniformity of pixel value of the subtracted images in the vertical dual-exposure PR method.
4. Vertical dual-exposure PR method with vertical magnification correction has the potential to provide higher quality merged PR images than the method without correction.

References

1. Paatero YV (1949) A new tomographical method for radiographing curved outer surfaces. Acta Radiol 32, 177-184.
2. Paatero YV (1954) Pantomography in theory and use. Acta Radiol 41, 321-335.
3. McDavid WD, Langlais RP, Welander U, Morris CR (1983) Real, double, and ghost images in rotational panoramic radiography. Dentomaxillofac Radiol 12, 122-128.
4. Kaugars GE, Collett WK (1987) Panoramic ghosts. Oral Surg Oral Med Oral Pathol 63, 103-108.
5. Reuter I, Ritter W, Kaeppler G (1999) Triple images on panoramic radiographs. Dentomaxillofac Radiol 28, 316-319.
6. Perschbacher S (2012) Interpretation of panoramic radiographs. Aust Dent J 57 Suppl 1, 40-45.
7. Hamedani S, Farshidfar N (2020) The practice of oral and maxillofacial radiology during COVID-19 outbreak. Oral Radiol 36, 400-403.
8. Little R, Howell J, Nixon P (2020) COVID-19 and beyond: Implications for dental radiography. Br Dent J 229, 105-109.
9. Meng L, Hua F, Bian Z (2020) Coronavirus disease 2019 (COVID-19): Emerging and future challenges for dental and oral medicine. J Dent Res 99, 481-487.
10. MacDonald DS, Colosi DC, Mupparapu M, Kumar V, Shintaku WH, Ahmad M (2021) Guidelines for oral and maxillofacial imaging: COVID-19 considerations. Oral Surg Oral Med Oral Pathol Oral Radiol 131, 99-110.
11. Kato M, Asakura S, Kimoto H, Sasaki T, Dezawa K, Amemiya T, Matsumoto K, Arai Y (2023) Reduction of ghost images of cervical vertebrae in panoramic radiography using vertical dual exposure. J Oral Sci (in press)
12. Matsuki T (1994) Basic study of one-shot dual-energy subtraction sialography: (ⅲ) fundamental study of contrast media. Oral Radiol 10, 55-62.
13. Workman A, Cowen AR (1995) Improved image quality utilizing dual plate computed

radiography. Br J Radio l68, 182-188.

14. Tsuda N, Tanaka N, Akasaka T, Yabuuchi H, Morishita J (2014) Dose reduction in general radiography for adult patients by use of a dual-side-reading photostimulable phosphor plate in a computed radiography system. Radiol Phys Technol 7, 310-315.
15. Imanishi Y, Sekiguchi T, Kato M, Kimoto H, Amemiya T, Dezawa K, Amemiya T, Matsumoto K, Arai Y (2023) Reduction of scratch or dirt artifacts on intraoral radiographs using dual imaging plates in image processing. Oral Radiol 39, 386-393.
16. Minato K, Yamazaki M, Yagi T, Hirata T, Tominaga M, You K, Ishikawa H (2023) Effectiveness of one-shot dual-energy subtraction chest radiography with flat-panel detector in distinguishing between calcified and non-calcified nodules. Sci Rep 13, 9548.
17. Sekiguchi T, Kato M, Kimoto H, Amemiya T, Dezawa K, Imanishi Y, Matsumoto K, Arai Y (2023) Correction of intraoral radiography with dual imaging plates using enlargement of the horizontal direction with division into 12 blocks. J Oral Sci 65, 40-43.
18. Farman AG, Farman TT (1998) Panoramic dental radiography using a charge-coupled device receptor. J Digit Imaging 11, 166-168.
19. Farman TT, Farman AG (1998) Clinical trial of panoramic dental radiography using a CCD receptor. J Digit Imaging 11, 169-171.
20. Ogawa K, Langlais RP, McDavid WD, Noujeim M, Seki K, Okano T, Yamakawa T, Sue T (2010) Development of a new dental panoramic radiographic system based on a tomosynthesis method. Dentomaxillofac Radiol 39, 47-53.
21. Noujeim M, Prihoda T, McDavid WD, Ogawa K, Yamakawa T, Seki K, Okano T, Sue T, Langlais RP (2011) Pre-clinical evaluation of a new dental panoramic radiographic system based on tomosynthesis method. Dentomaxillofac Radiol 40, 42-46.

Tables and Figures

Table 1. TMV and MMV, and error when merged by the least squares method at each tilt angle and height

Tilt angle	0°			10°			20°			30°		
Height of X-ray focus	TMV	MMV	Error (%)	TMV	MMV	Error (%)	TMV	MMV	Error (%)	TMV	MMV	Error (%)
5 mm	1.0000	0.9980	0.20	0.9978	0.9980	−0.02	0.9954	0.9970	−0.16	0.9928	0.9940	−0.12
10 mm	1.0000	0.9980	0.20	0.9956	0.9950	0.06	0.9909	0.9930	−0.21	0.9855	0.9890	−0.35
15 mm	1.0000	0.9970	0.30	0.9934	0.9950	−0.16	0.9863	0.9880	−0.17	0.9783	0.9790	−0.07
20 mm	1.0000	0.9990	0.10	0.9912	0.9930	−0.18	0.9817	0.9830	−0.13	0.9710	0.9730	−0.20

TMV, theoretical magnification value; MMV, measured magnification value

The error is a subtraction of the MMV from the TMV.

Table 2 Standard deviations of the pixel value of subtraction images before and after vertical magnification correction at each tilt angle and height of the X-ray focus

Tilt angle	0°		10°		20°		30°	
Height of X-ray focus	VMC-	VMC+	VMC-	VMC+	VMC-	VMC+	VMC-	VMC+
5 mm	6.24	5.33	6.50	5.73	8.69	6.07	10.79	7.42
10 mm	7.00	5.81	9.03	6.61	13.70	6.00	18.59	7.47
15 mm	7.32	5.78	11.66	6.83	19.12	5.54	26.33	6.99
20 mm	7.36	5.99	14.86	7.23	23.04	6.55	31.68	7.26

VMC-, before vertical magnification correction; VMC+, after vertical magnification correction

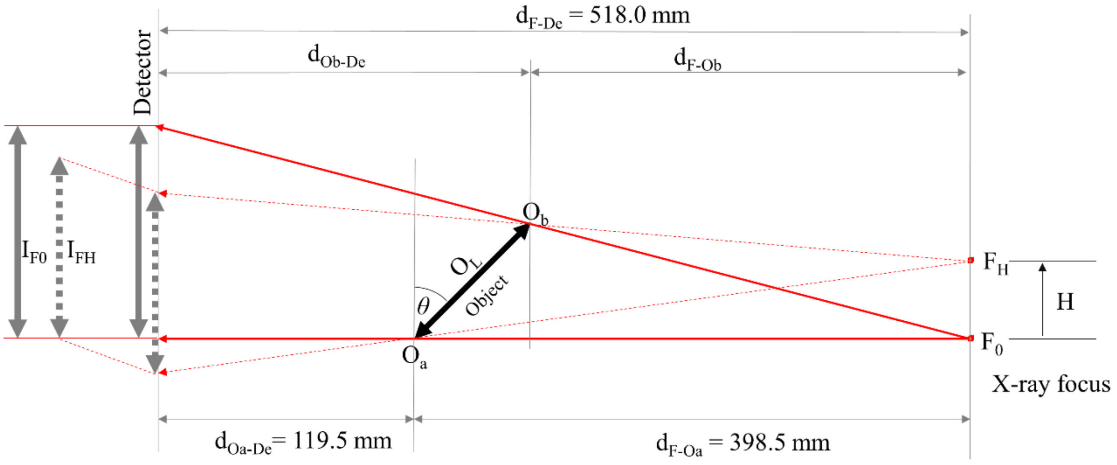

Fig. 1 The size of the object projected on the detector with the X-ray focus at an elevation of H, and the object tilted at an angle of θ

F_0, X-ray focus and detector at original position; F_H, X-ray focus and detector at position raised by H mm; H, height of X-ray focus and detector; I_{F0}, image length taken at F_0; I_{FH}, image length taken at F_H; O_a, a-point of the object (incisal edge); O_b, b-point of the object (apex), O_L, object length (distance between O_a and O_b); $d_{F\text{-}De}$, horizontal distance between F and detector; $d_{F\text{-}Oa}$, horizontal distance between X-ray focus and O_a; $d_{Oa\text{-}De}$, horizontal distance between O_a and detector; $d_{F\text{-}Ob}$, horizontal distance between X-ray focus and O_b; $d_{Ob\text{-}De}$, horizontal distance between O_b and D_e; θ, tilt angle of the object

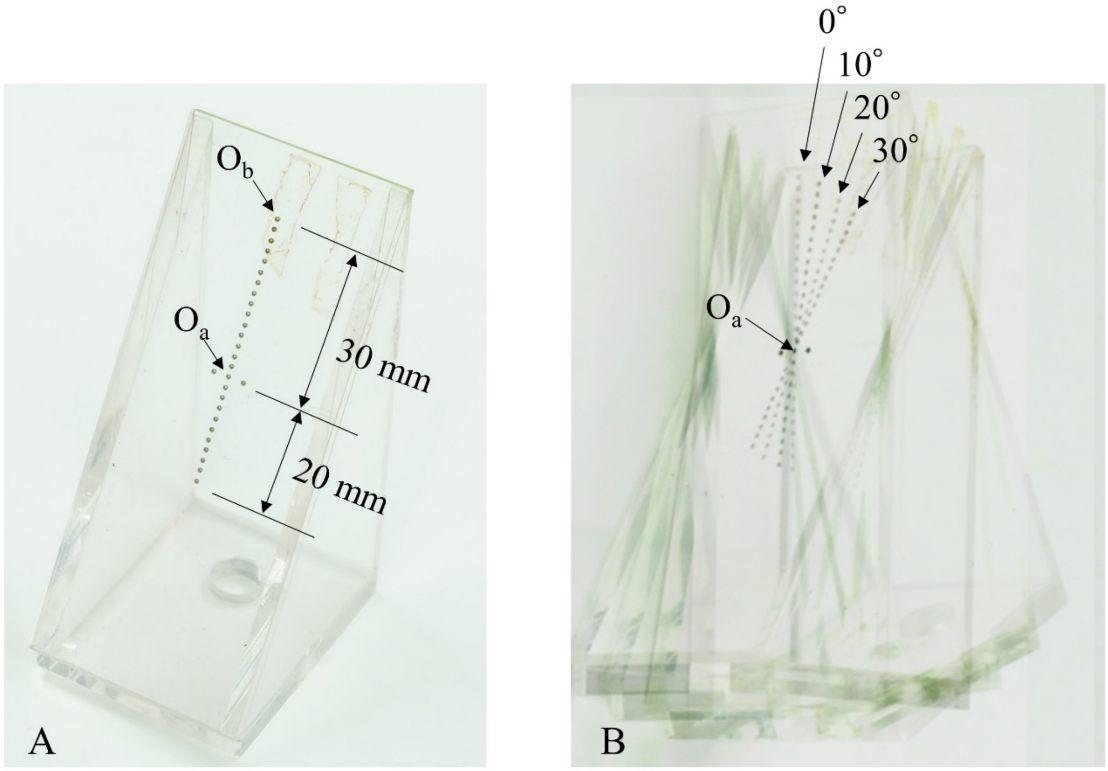

Fig. 2 Steel ball phantom

A: Overview of the steel ball phantom

Steel balls 0.5 mm in diameter were embedded in a 50-mm-long acrylic plate at intervals of 2 mm. The center position was defined as a position 30-mm below the top of the uppermost steel ball (O_a). The uppermost steel ball was designated as O_b.

B: The image merged from photographs taken from 0°to 10°, 20°, and 30° with the O_a as the center.

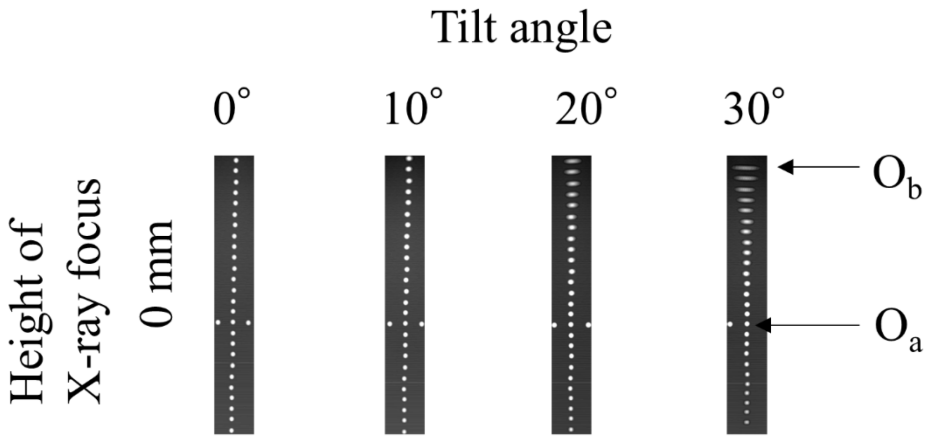

Fig. 3 Cropped panoramic radiographs of the steel ball phantom at X-ray focus height of 0 mm and four tilt angles

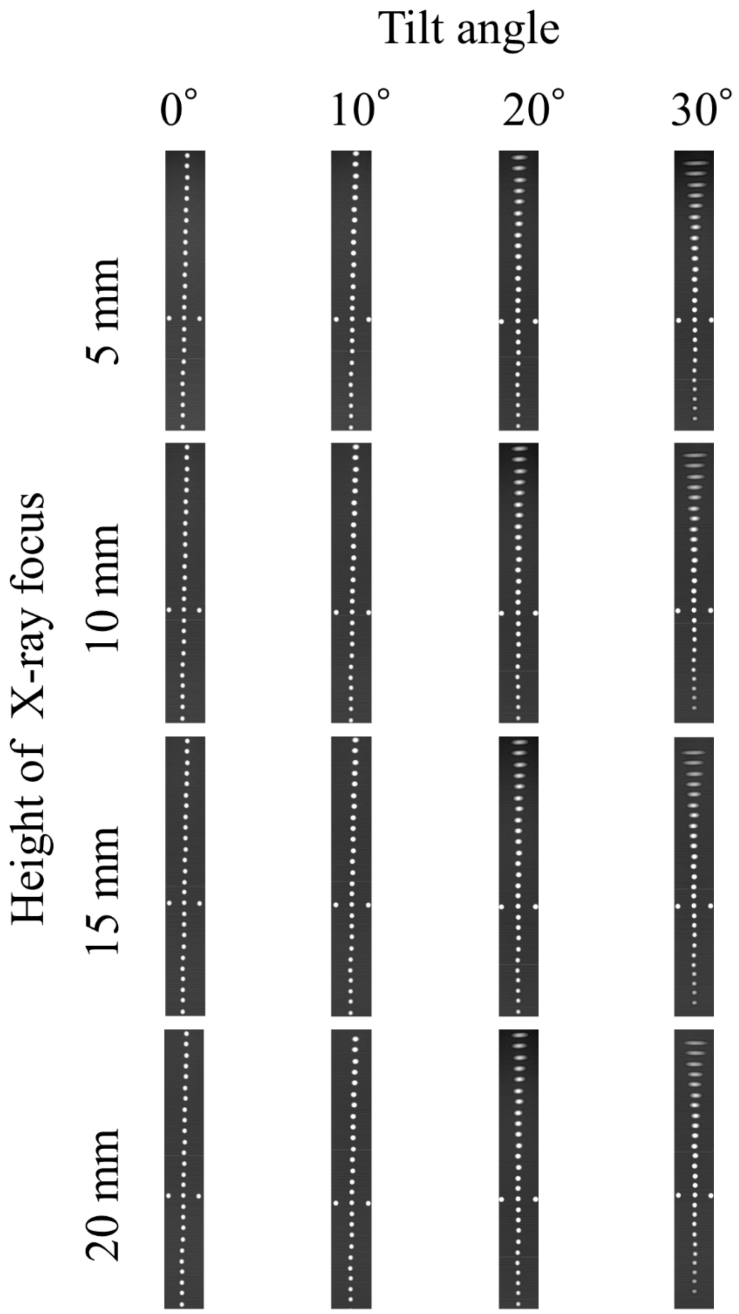

Fig. 4 Cropped panoramic radiographs of the steel ball phantom at X-ray foci of 5, 10, 15, and 20 mm and four tilt angles

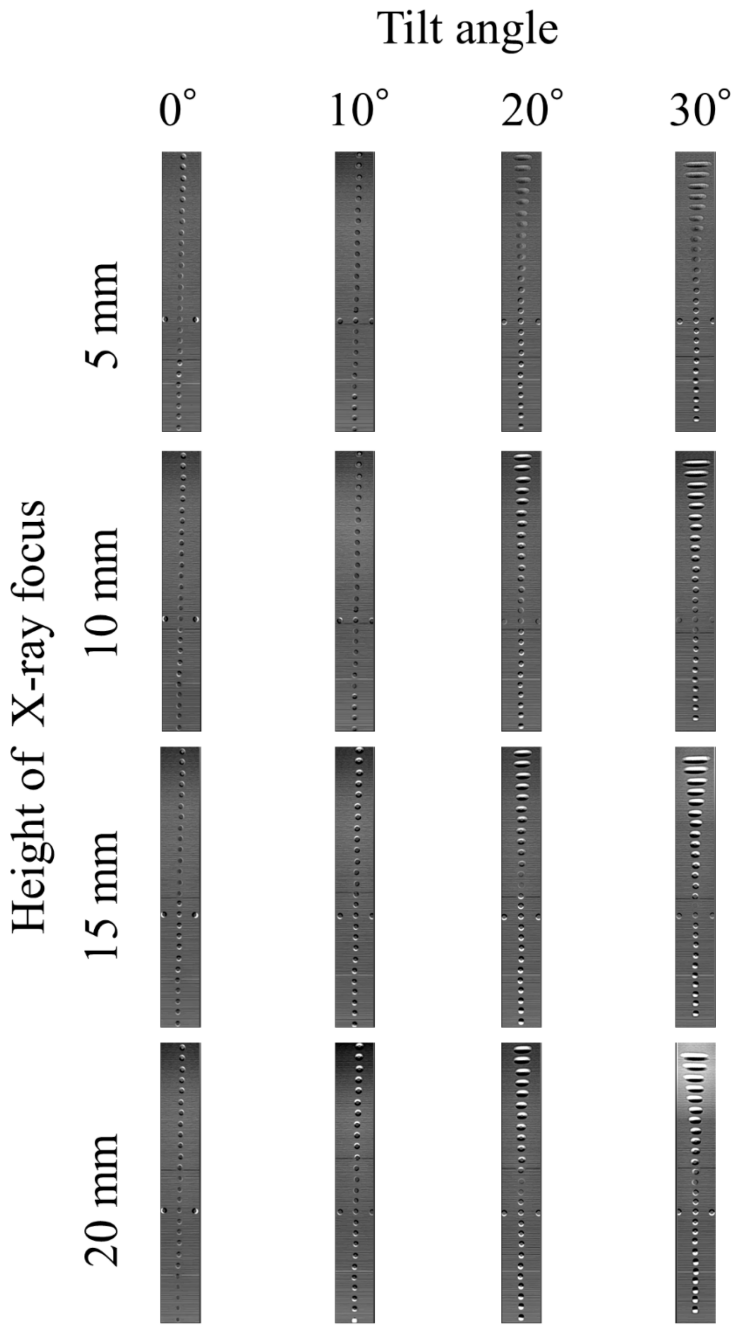

Fig. 5 Subtracted images between the images taken at F_0 and F_H at each tilt angle

F_0, X-ray focus and detector at original position (0 mm); F_H, X-ray focus and detector at a height of H mm from F_0

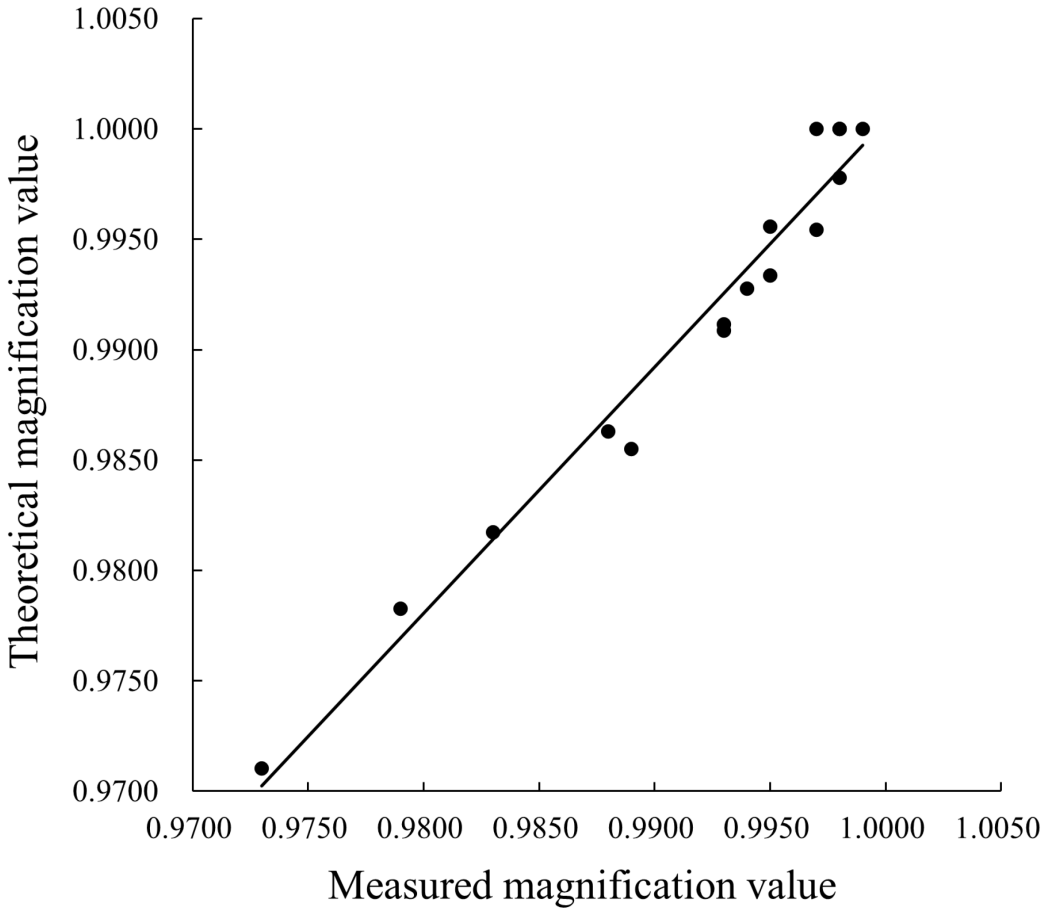

Fig. 6 Regression line between the theoretical magnification values and the measured magnification values in the vertical direction

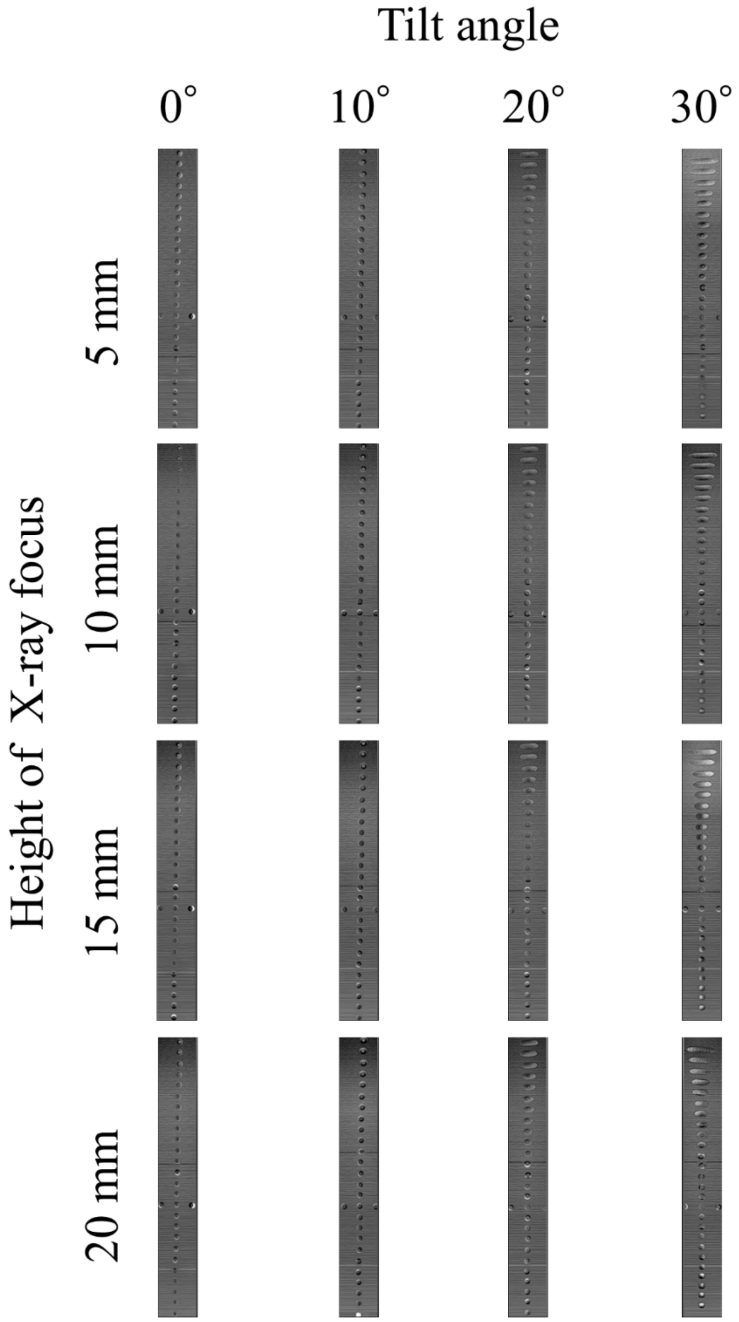

Fig. 7 Subtracted images between the images taken at F_0 and images with vertical magnification correction at F_H at each tilt angle

F_0, X-ray focus and detector at original position (0 mm); F_H, X-ray focus and detector at a height of H mm from F_0

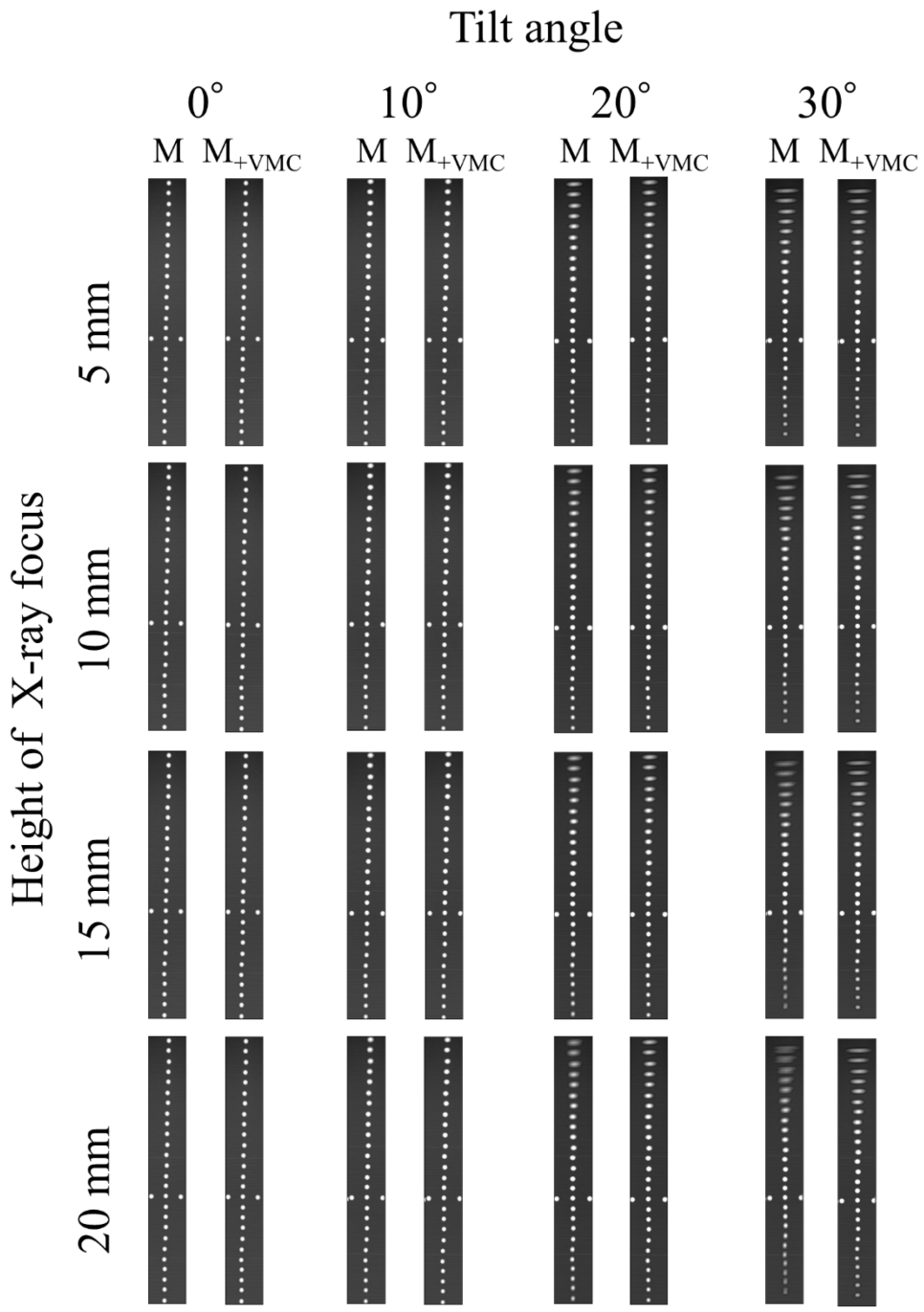

Fig. 8 Merged images before and after vertical magnification correction at each tilt angle

M, merged image; M_{+VMC}, merged image with magnification correction

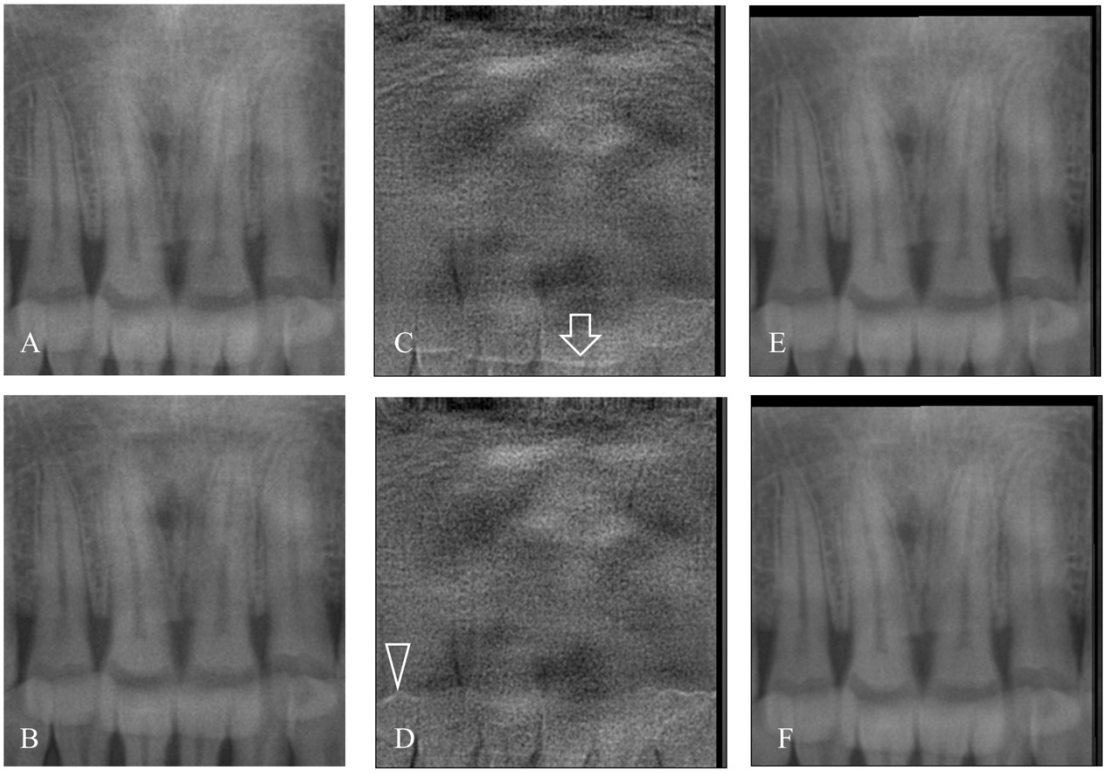

Fig. 9 Vertical magnification correction in the human head phantom

A: Cropped panoramic radiographs of the human head phantom taken at a height of 0 mm

B: Cropped panoramic radiographs of the human head phantom taken at a height of 20 mm

C: Subtracted image from Fig. 9A to Fig. 9B

D: Subtracted image from Fig. 9A to Fig. 9B with vertical magnification correction

E: Merged images

F: Merged images with vertical magnification correction

The horizontal radiopaque lines on the incisal edge of the maxillary incisors in C (arrow) disappeared after vertical magnification correction as shown in D. The incisal edge of the mandibular canine became visible in D (arrowhead) after vertical magnification correction.